THE JOURNAL OF PHYSICAL CHEMISTRY Letters

Letter

Cite This: J. Phys. Chem. Lett. 2019, 10, 4794−4799

pubs.acs.org/JPCL

Revealing Insights into Li_xFePO_4 Nanocrystals with Magnetic Order at Room Temperature Resulting in Trapping of Li Ions

Jiangtao Hu,[†,⊥] Hua Zeng,[†,⊥] Xin Chen,[†] Ziqi Wang,[†] HongBin Wang,[†] Rui Wang,[†] Lijun Wu,[‡] Qingzhen Huang,[§] Lingyong Kong,[∥] Jiaxin Zheng,[†] Yinguo Xiao,*[,†] Wei Zhang,*[,‡] and Feng Pan*[,†]

[†]School of Advanced Materials, Peking University, Shenzhen Graduate School, Shenzhen 518055, China

[‡]Sustainable Energy Technologies Department, Brookhaven National Laboratory, Upton, New York 11973, United States

[§]NIST Center for Neutron Research, National Institute of Standards and Technology, 100 Bureau Drive, Gaithersburg, Maryland 20899, United States

[∥]Dynanonic Co., Ltd., Shenzhen 518055, People's Republic of China

Supporting Information

ABSTRACT: A systematic study on the structures, magnetic properties, and electrochemical performance of Li_xFePO_4 was carried out. Interestingly, it was found that the magnetic phase transition temperature is around 295 K in Li_xFePO_4 ($x \leq 0.12$) nanocrystals, which is higher than that of $LiFePO_4$ (T_N = 51(1) K) and $FePO_4$ (T_N = 114(1) K) phases. The origin of magnetic order around room temperature (RT) in Li_xFePO_4 ($x \leq 0.12$) is proposed to be due to both Fe^{2+}−Fe^{3+} superexchange and the broken local symmetries induced by Fe^{2+}−Li^+ antisite defects. Ab initio calculations were adopted to calculate the total energy change of the ferromagnetic state and antiferromagnetic state (ΔE) to qualitatively estimate T_N and proved the existence of the magnetic order around room temperature. Because of the strong Lorentz force in RT magnetic domains, Li ions will be trapped and form sub-10 nm solid solution domains of $Li_{0+\delta}FePO_4$, which have a direct relationship with electrochemical performance during (de)lithiation procedures.

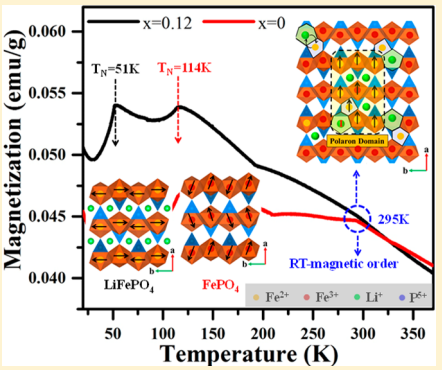

Magnetoelectrochemistry remains relatively unfamiliar to us, although it has been researched for many years.[1] Magnetic fields have assignable influence on electrochemistry, including three aspects: mass transport, electrode kinetics and deposit morphology.[2−4] Li-containing transition metal (TM) compounds are usually employed as cathode materials for lithium-ion batteries (LIBs), such as olivine $LiFePO_4$, traditional $LiCoO_2$, and the emerging multication layered $LiNi_{1-x}(MnCo)_xO_2$ (generally called NMC). In these materials, the TM cations [Ni(II/III), Co(II/III), and Mn(II/III/IV)] usually contain unpaired spin electrons, hence indicating strong magnetic interactions. Via neutron scattering and magnetic measurements, many works have been carried out to study the magnetic properties in the above cathode materials.[5−13] However, nearly all the previous studies focused on only the magnetic structures and properties, and few works pay attention to the relationship between the magnetic properties and the electrochemical performance in TM compound cathode materials.

Actually, given that the electronic structure of a substance is intimately related to the magnetic properties, the magnetic measurement can act as an effective probe toward understanding not only the magnetism but also the atomic details of certain substances.[14,15] The magnetic measurements enable detection of the variation of magnetic signals associated with the local structural changes and, more importantly, the emergence of new magnetic signals originating from a small amount of magnetic substance with high sensitivity. This technique has been applied to investigate the magnetic properties and electronic structures in various LIB electrode materials.[14,15]

$LiFePO_4$ with olivine structure has been commercially used as a high-rate cathode for LIBs.[16,17] Magnetic ordering in these electrodes mostly occurs at low temperatures. For example, antiferromagnetic behavior has been observed below 51(1) K in $LiFePO_4$ and below 114(1) K in $FePO_4$.[15,18,19] During the redox reaction in Li_xFePO_4, a redox couple of Fe^{2+}/Fe^{3+} will be generated, and the magnetic exchange interactions between magnetic ions Fe^{3+} and Fe^{2+} have to be taken into account. It is known that electron configurations of Fe^{3+} and Fe^{2+} are d^5 and d^6, respectively, and the splitting of the d-orbitals of Fe ions will occur and give rise to doubly degenerate e_g orbitals and triply degenerate t_{2g} orbitals within the framework of the FeO_6 octahedra. The 5 spins of electrons (2 e_g spins and 3 t_{2g} spins) in Fe^{3+} will align in the same direction, realizing a high-spin state, whereas the extra spin of the electron in Fe^{2+} will point in

Received: May 30, 2019
Accepted: August 7, 2019
Published: August 7, 2019

DOI: 10.1021/acs.jpclett.9b01557
J. Phys. Chem. Lett. 2019, 10, 4794−4799

the opposite direction from other spins. Because the exchange interaction between Fe^{2+} and Fe^{3+} is achieved through the electron transfer, the electron can hop back and forth between Fe^{2+} and Fe^{3+} via the O 2p state only if both ions are aligned ferromagnetically. As a consequence, the ferromagnetic state emerges.[20] It is different from the magnetic state of $LiFePO_4$ and $FePO_4$, in which exchange interactions of Fe^{2+}−Fe^{2+} and Fe^{3+}−Fe^{3+} favor antiferromagnetic coupling of Fe ions with different strengthens, resulting in different magnetic transition temperatures.[18]

In this Letter, we present the first comprehensive study on the structural and magnetic properties Li_xFePO_4 over a wide range of Li concentrations and correlate them with the electrochemical performance by using X-ray diffraction (XRD), neutron powder diffraction (NPD), high-resolution transmission electron microscopy (HRTEM) imaging, and magnetic measurements at temperatures between 5 and 300 K. Interestingly, the magnetic state of Li_xFePO_4 ($x \leq 0.12$) at room temperature (RT) was found, associated with the formation of magnetic polaron domains, which is different from $LiFePO_4$ and $FePO_4$. The new magnetic phase results in the trapping of Li ions and formation of solid solution $Li_{0+\delta}FePO_4$ domains (~10 nm) in local regions of the matrix $FePO_4$ phase. We also discuss the origin of the RT magnetism order phase and its impact on the transport properties of Li ions in Li_xFePO_4.

Several samples of Li_xFePO_4 ($0 \leq x \leq 1$) were obtained by chemical delithiation of pristine $LiFePO_4$ (see the Supporting Information). Only two sets of diffraction peaks related to $LiFePO_4$ and $FePO_4$ phases were observed in the XRD patterns of all the samples, as shown in Figure 1a. The fitting

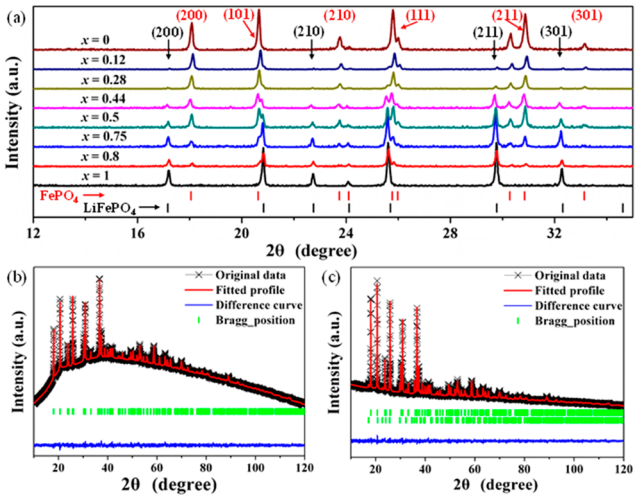

Figure 1. $LiFePO_4$/$FePO_4$ two-phase system in a series of Li_xFePO_4 samples ($0 \leq x \leq 1$) at the electrode scale. (a) XRD patterns of Li_xFePO_4 and (b and c) Rietveld refinement results of $FePO_4$ and $Li_{0.12}FePO_4$, respectively, obtained by Fullprof program, showing no impurity phase was detected.

results by the Fullprof program of Li_xFePO_4 are shown in Figures 1b,c and S1, further indicating that no impurity phase was detected in all the samples. SEM images of Li_xFePO_4 show that the particle size is in the range of 200−600 nm (Figure S2). The electrochemical performance of $LiFePO_4$ is shown in Figures S3 and S4, including discharge specific capacity (~160 mAh g^{-1} at 0.1C) and rate performance (~71 mAh g^{-1} at 10C).

A systematic magnetic measurement on Li_xFePO_4 nanocrystals was carried out as shown in Figure 2.The magnetic

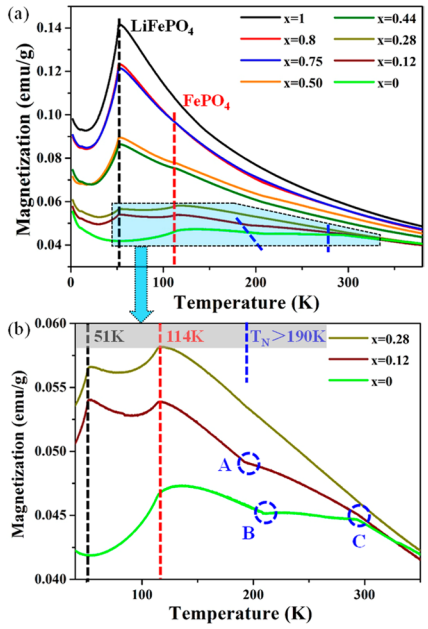

Figure 2. (a) Temperature dependence of the magnetic susceptibility of Li_xFePO_4 ($0 \leq x \leq 1$). (b) Detailed magnetic susceptibility of $Li_{0.28}FePO_4$, $Li_{0.12}FePO_4$, and $FePO_4$, corresponding to the shaded section in panel a. Continuous transitions at T_N greater than 190 K (a range between points A and C in $Li_{0.12}FePO_4$ or points B and C in $FePO_4$ labeled by dashed circles).

transition Néel temperature (T_N) of $LiFePO_4$ phase was clearly detected at 51(1) K in all nanocrystals, which is the same as in previous reports,[14,21,22] except the fully delithiated $FePO_4$ sample. Once the delithiation started, a transition at about 114(1) K was observed in the magnetization curves, corresponding to the $FePO_4$ phase (Figure 2a).[19] Interestingly, new anomalous magnetic phases were observed in the magnetization curves of $Li_{0.12}FePO_4$ and $FePO_4$ nanocrystals near RT (Figure 2b). In the magnetization curve of $Li_{0.12}FePO_4$ nanocrystals (Figure 2b), two kinks are observed at both 190 K (point A) and 295 K (point C), as highlighted by two dashed circles. Such kinks became more significant in the magnetization curve of $FePO_4$, in which the first one at 215 K is due to the overlay effect (Figure S5), whereas the second one at 295 K represents a magnetic phase transition originated from a new magnetic phase other than $LiFePO_4$ and $FePO_4$. The new magnetic transition temperature is different from the magnetic phase transition of impurity phases that might form during sample synthesis, such as α-Fe_2O_3 (T_N = 950 K)[23] and Fe_3O_4 (T_C = 860 K).[24] Although it seems that the T_C of Fe_2P (T_C = 216 K) is close to point B,[25] Fe_2P can be formed only when the reaction temperature reaches 800 °C during the synthesis process.[26,27] However, no magnetic transition at 216 K was detected in the pristine sample $LiFePO_4$ (Figure 2a), and furthermore, the chemical delithiation took place at RT, thus eliminating the possibility of forming the impurity Fe_2P phase during delithiation. Therefore, our results cannot be explained by the presence of Fe_2P. No impurity phase was formed in all samples (Figures 1b,c and S1), so the new anomalous magnetic phases appearing near RT come totally from Li_xFePO_4. Although it is impossible to unambiguously

DOI: 10.1021/acs.jpclett.9b01557
J. Phys. Chem. Lett. 2019, 10, 4794−4799

determine the magnetic structure RT order phase, magnetic measurement demonstrates that there must be a high magnetic transition temperature around RT.

To measure magnetic properties and the concentrations of structural defects, NPD was performed on $FePO_4$ and $LiFePO_4$ nanocrystals (Figure 3). The refinement results indicate that

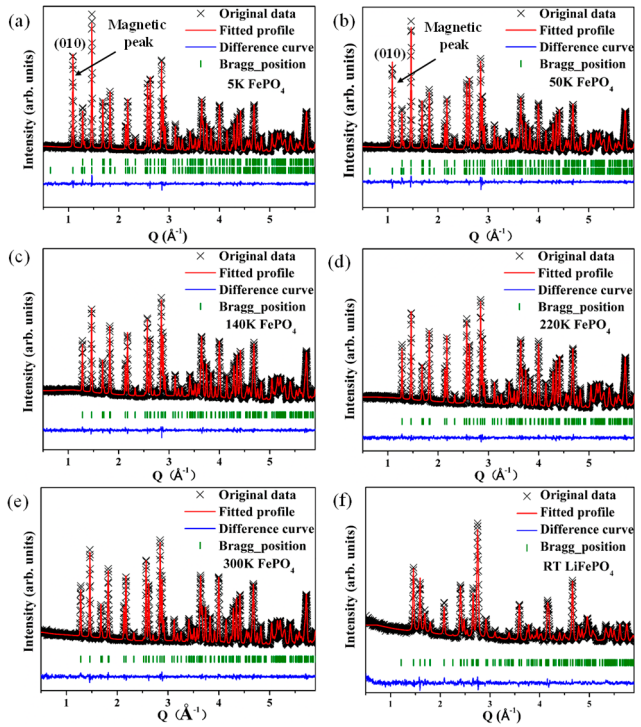

Figure 3. Neutron powder diffraction patterns of $FePO_4$ and $LiFePO_4$. (a–e) Rietveld refinement results of $FePO_4$ at different temperatures, indicating the existence of about 0.3% Fe^{2+}–Li^+ antisite defects. The (010) magnetic reflection was observed only at 5 and 50 K. (f) Rietveld refinement result of $LiFePO_4$ at RT, indicating the existence of about 0.4% Fe^{2+}–Li^+ antisite defects.

the concentrations of Fe^{2+}–Li^+ antisite defects in $LiFePO_4$ and $FePO_4$ are about 0.3% and 0.4% with about 0.1% simulation error, respectively (Tables S1 and S2-5). In $FePO_4$ nanocrystals, the integrated intensity of (010) magnetic reflection can be considered as a magnetic order of the Fe^{3+} moments, which was observed at 5 and 50 K (Figure 3a and b). As for the neutron diffraction patterns collected above the T_N of $FePO_4$ and in $LiFePO_4$ at RT (Figure 3c–f), all reflections can be properly indexed as nuclear reflections of $FePO_4$ or $LiFePO_4$ phase, but no extra magnetic peak was observed. Therefore, it is difficult to identify the magnetic reflection through the NPD measurements. This may result from the RT magnetic order domain being too small to be detected.

What is the origin of RT-magnetic order in Li_xFePO_4 ($x \leq 0.12$) nanocrystals? Considering the combined measurements of NPD and magnetization characterization, the RT-magnetic order could be attributed to Fe^{2+}–Li^+ antisite defects at high delithiation state. The mechanism of generating RT-magnetic order in the high delithiation state of $LiFePO_4$ is proposed in Figure 4. It has been claimed that the difference between magnetic properties of $FePO_4$ and $LiFePO_4$ can be attributed to the different properties of Fe ions, i.e., strong anisotropy of Fe^{2+} in $LiFePO_4$ and isotropy of Fe^{3+} in $FePO_4$.[18] The magnetic structures of these two materials are proposed as

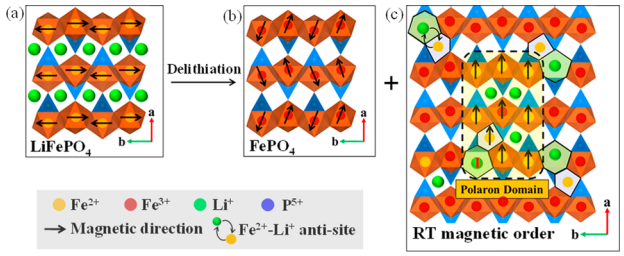

Figure 4. Schematic illustration of the origin of room-temperature magnetism at high delithiation state of Li_xFePO_4. (a) Magnetic structure of $LiFePO_4$ showing antiferromagnetic behavior. (b and c) Magnetic structures of $FePO_4$ and RT magnetic order zone after delithiation, respectively. While $FePO_4$ still possesses an antiferromagnetic structure, similar to that of $LiFePO_4$, a ferromagnetic-like state is formed in the RT magnetic order zone because of the RT magnetic order within the magnetic polaron domain marked by a dashed black box, which is caused by the presence of Fe^{2+}–Li^+ antisite defects and superexchange between Fe^{2+} and Fe^{3+}.

shown in panels a and b of Figure 4, respectively. There are about 0.4% Fe^{2+}–Li^+ antisite defects in $FePO_4$ nanocrystals detected by NPD in the present work, which may aggregate in local regions with the higher concentration, as observed in the previous work.[28] Therefore, the local symmetry should be broken at the Fe^{2+}–Li^+ antisite defects. Consequently, the adjacent antiferromagnetic interaction between nearby Fe^{2+} ions would be broken, causing the formation of a ferromagnetic-like state and local magnetic ordering as illustrated in Figure 4c. More importantly, at a high delithiation state, Li_xFePO_4 ($0 \leq x \leq 0.12$) contains mixed valence states of Fe^{3+} and Fe^{2+}, indicating the existence of not only Fe^{3+}–Fe^{3+} superexchange but also the Fe^{2+}–Fe^{3+} superexchange that may lead to the formation of magnetic polaron domains (Figure 4c).[29] The superexchange interaction in the polaron domain is large enough (few tenths of an electronvolt) to enable the magnetic order at RT.[20] Therefore, both the local symmetries broken at Fe^{2+}–Li^+ antisite defects and Fe^{2+}–Fe^{3+} superexchange might play a dominate role in generating the magnetic state of Li_xFePO_4 ($x \leq 0.12$) at RT.

Ab initio calculations were further employed to verify the origin of magnetic order around RT at the high delithiation state of Li_xFePO_4 ($x \leq 0.12$). The magnetic transition Néel temperature has a positive correlation with the total energy change of the paramagnetic state and antiferromagnetic state. However, it is too hard to relax atomic positions and cell parameters of the paramagnetic state. For some traditional materials, there is also a positive correlation between the total energy change of the paramagnetic state and antiferromagnetic state and the total energy change of the ferromagnetic state and antiferromagnetic state.[30] Thus, we can compare the total energy change of the ferromagnetic state and antiferromagnetic state (ΔE) to qualitatively estimate T_N. The total energy of $Li_{1-x}FePO_4$ with 0, 12.5%, and 25% Fe^{2+}–Li^+ antisite defects is shown in Table S3.

As shown in Figure 5a, for $Li_{1-x}FePO_4$ without any Fe^{2+}–Li^+ antisite defects, ΔE gradually increases with the increase of x. ΔE of $LiFePO_4$ and $FePO_4$ are 0.076 and 0.4 eV, respectively, indicating that T_N of $FePO_4$ is greater than T_N of $LiFePO_4$, which coincides with the experimental result. When Fe^{2+}–Li^+ antisite defects arise, the local symmetry will be broken. During delithiation of $LiFePO_4$ with 25% Fe^{2+}–Li^+ antisite defects, there is a new antiferromagnetic state with a lower total energy

DOI: 10.1021/acs.jpclett.9b01557
J. Phys. Chem. Lett. 2019, 10, 4794–4799

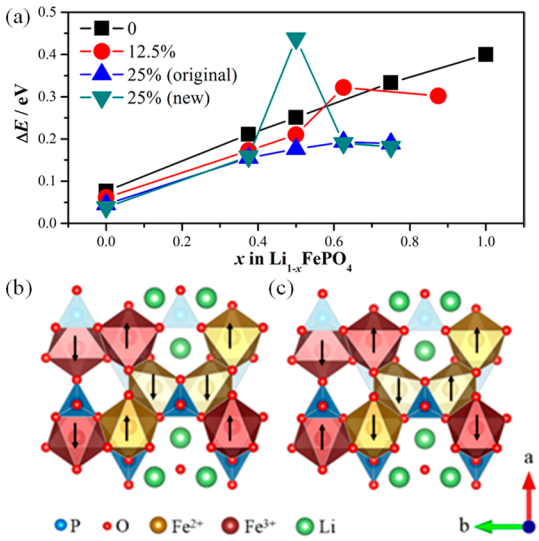

Figure 5. (a) ΔE during delithiation of $LiFePO_4$ with 0, 12.5%, and 25% Fe^{2+}−Li^+ antisite defects. The original ΔE is based on the original antiferromagnetic state which is same as the antiferromagnetic state without any Fe^{2+}−Li^+ antisite defects. The new ΔE is based on the new antiferromagnetic state formed by the Fe^{2+}−Fe^{3+} superexchange. Schematics for structures of $Li_{0.5}FePO_4$ with 25% Fe^{2+}−Li^+ antisite defects: (b) the original antiferromagnetic state and (c) the new antiferromagnetic state.

due to the Fe^{2+}−Fe^{3+} superexchange, which leads to a higher ΔE. The structures of the original and the new antiferromagnetic state are shown in Figure 5b,c. For $Li_{1-x}FePO_4$ with 25% Fe^{2+}−Li^+ antisite defects, the new ΔE increases first and then decreases with the increase of x (Figure 5a). When x is 0.5, the new ΔE reaches a maximum value (0.438 eV), higher than the ΔE of $FePO_4$. Therefore, it can be inferred that T_N in Li_xFePO_4 ($x \leq 0.12$) is greater than T_N of $FePO_4$ when Fe^{2+}−Li^+ antisite defects in Li_xFePO_4 ($x \leq 0.12$) aggregate to a certain concentration. One may suspect that only 0.4% Fe−Li antisite defects are experimentally detected, but the concentrations in local regions may reach 25%. When the two different structures of $LiFePO_4$ with the same proportion of Fe^{2+}−Li^+ antisite defects are compared (Figure S6), the total energy of the structure in which Fe^{2+}−Li^+ antisite defects gather together is lower, indicating that Fe^{2+}−Li^+ antisite defects tend to gather in local regions.

Forming a RT-magnetic order region in Li_xFePO_4 ($x \leq 0.12$) nanocrystals may impact the performance of $LiFePO_4$ in Li-ion batteries, so we carried out HRTEM testing on Li_xFePO_4 ($x \leq 0.28$) nanocrystals. Although the XRD measurements identified only two phases of $LiFePO_4$ and $FePO_4$ formed at the electrode scale, the localized phase transformation within a single nanocrystal particle involves the formation of a solid solution phase, as evidenced by HRTEM images (Figure 6). The localized areas marked by white boxes in Figure S7 were used to obtain the HRTEM images of $FePO_4$, $Li_{0.12}FePO_4$, and $Li_{0.28}FePO_4$ as shown in panels a, b, and c of Figure 6, respectively. The lattice displacement in the HRTEM images was measured by geometric phase analysis (GPA) and then converted to Li concentrations in Figure 6d−f, following the procedure reported in previous work.[31] Only two phases of $FePO_4$ (blue in Figure 6d) and $LiFePO_4$ (red in Figure 2d) were detected in the local area of a $Li_{0.28}FePO_4$ single nanocrystal particle, which is consistent with the XRD

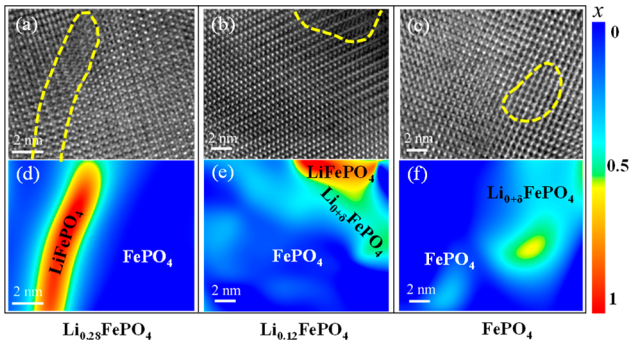

Figure 6. Localized solid solution phase $Li_{0+\delta}FePO_4$ in single particles. HRTEM images of (a) $Li_{0.28}FePO_4$, (b) $Li_{0.12}FePO_4$, and (c) $FePO_4$, obtained from the local regions as marked by white boxes in Figure S7. (d, e, and f) Phase distribution and variation of Li concentration (x in Li_xFePO_4) corresponding to panels a, b, and c, respectively, showing the existence of solid solution phase $Li_{0+\delta}FePO_4$ in local regions. Color scale indicates Li concentration x.

results in Figure 1a. However, besides the two phases, solid solution domains of $Li_{0+\delta}FePO_4$ ($0.2 < \delta < 0.7$) were formed at the interface between $FePO_4$ and $LiFePO_4$, when the Li concentration of the whole particle was reduced to 0.12 (Figure 6e). The domain size is around 5 nm. While the particle was further delithiated to be a $FePO_4$ nanocrystal, the $LiFePO_4$ phase was completely absent (Figure 6f). The solid solution phase of $Li_{0+\delta}FePO_4$ was still locally formed within the matrix of $FePO_4$, but it possessed a different range of Li concentration ($0.3 < \delta < 0.6$). Therefore, the localized structural transformation cannot be simply described by a pure model of a two-phase transition. The nanoscale $Li_{0+\delta}FePO_4$ phase has been observed in chemically delithiated particles by scanning X-ray diffraction microscopy (SXDM) measurements, which may be stabilized by inducing coherency strain at certain interfaces.[32] However, the sub-10 nm solid solution domains can only be observed locally using the current imaging technique and are inaccessible to XRD and SXDM measurements. Although, Li_xFePO_4 ($x \leq 0.12$) locates at the full delithiation state, no Li ions could be further extracted after full chemical or electrochemical delithiation; the solid solution phase $Li_{0+\delta}FePO_4$ still exists as nanoscale domains with a size of 5 nm. In other words, Li ions are blocked in the Li_xFePO_4 ($x \leq 0.12$) nanocrystal (labeled as Li(I) in Figure 4c), which are difficult to migrate out of the crystal structure because of an internal magnetic field of RT magnetic order domains with Lorentz force. White and co-workers carried out investigations of magnetoelectrochemical effects at ultramicroelectrodes, which proved the role of the magnetic field effecting an electrified body.[33−35] Hence, the RT magnetic order domains prohibiting some amount of Li ions could be expected to degrade the energy capacity of $LiFePO_4$ during the charge−discharge process.

In summary, we performed a systematic study on the structures and magnetic properties of Li_xFePO_4 by combining GPA, XRD, NPD, HRTEM, and magnetic measurements and correlated them with the electrochemical performance in $LiFePO_4$. Two magnetic transitions were detected in the magnetization curve of Li_xFePO_4 ($0.28 \leq x \leq 1$), which correspond to $LiFePO_4$ and $FePO_4$ phases. In contrast to these common findings, an unexpected transition was revealed around 295 K in Li_xFePO_4 ($x \leq 0.12$) nanocrystals. We proposed that the existence of local symmetries broken at

DOI: 10.1021/acs.jpclett.9b01557
J. Phys. Chem. Lett. 2019, 10, 4794−4799

Fe^{2+}−Li^{+} antisite defects and Fe^{2+}−Fe^{3+} superexchange would be a dominant source of forming RT magnetism in the high delithiation state of Li_xFePO_4, which was proven by the final calculation result of energy change between the ferromagnetic state and antiferromagnetic state (ΔE). The RT magnetism can impact the Li-ion transport and capacities to degrade the performance of LIBs. This study is the first to report the magnetic ordering in Li_xFePO_4 ($x \leq 0.12$) during redox reaction at RT, offering a new insight into the physical and chemical processes that underlie the operation of batteries.

■ ASSOCIATED CONTENT

Supporting Information

The Supporting Information is available free of charge on the ACS Publications website at DOI: 10.1021/acs.jpclett.9b01557.

Details about experimental methods, calculation methods, Rietveld refinement results, SEM images, electrochemical performance, TEM images, and refined crystallographic parameters at different temperature (PDF)

■ AUTHOR INFORMATION

Corresponding Authors

*E-mail: panfeng@pkusz.edu.cn (F.P.).
*E-mail: zhangw@bnl.gov (W.Z.).
*E-mail: y.xiao@pku.edu.cn (Y.X.).

ORCID

Wei Zhang: 0000-0001-7031-162X
Feng Pan: 0000-0002-8216-1339

Author Contributions

⊥J.H. and H.Z. contributed equally to this work.

Notes

The authors declare no competing financial interest.

■ ACKNOWLEDGMENTS

This work was financially supported by National Key R&D Program of China (2016YFB0700600), the National Natural Science Foundation of China (Nos. 21603007 and 51672012), Soft Science Research Project of Guangdong Province (No. 2017B030301013), and Shenzhen Science and Technology Research Grant (No. JCYJ20160226105838578 ZDSYS201707281026184). Electron microscopy work was performed at the Center for Functional Nanomaterials, Brookhaven National Laboratory, which is supported by the U.S. Department of Energy (DOE), Office of Basic Energy Science, under contract DE-SC0012704.

■ REFERENCES

(1) Monzon, L. M. A.; Coey, J. M. D. Magnetic Fields in Electrochemistry: The Lorentz Force. A Mini-review. *Electrochem. Commun.* **2014**, *42*, 38−41.

(2) Fahidy, T. Z. Magnetoelectrolysis. *J. Appl. Electrochem.* **1983**, *13* (5), 553−563.

(3) Chia-Chien, L.; Chou, T.-C. Effects of Magnetic Field on the Reaction Kinetics of Electroless Nickel Deposition. *Electrochim. Acta* **1995**, *40* (8), 965−970.

(4) Shannon, J. C.; Gu, Z. H.; Fahidy, T. Z. Surface Morphology of Cathodic Nickel Deposits Produced via Magnetoelectrolysis. *J. Electrochem. Soc.* **1997**, *144* (12), L314−L316.

(5) Toft-Petersen, R.; Reehuis, M.; Jensen, T. B. S.; Andersen, N. H.; Li, J.; Le, M. D.; Laver, M.; Niedermayer, C.; Klemke, B.; Lefmann, K.; Vaknin, D. Anomalous Magnetic Structure and Spin Dynamics in Magnetoelectric $LiFePO_4$. *Phys. Rev. B: Condens. Matter Mater. Phys.* **2015**, *92*, 024404.

(6) Toft-Petersen, R.; Andersen, N. H.; Li, H.; Li, J.; Tian, W.; Bud'ko, S. L.; Jensen, T. B. S.; Niedermayer, C.; Laver, M.; Zaharko, O.; Lynn, J. W.; Vaknin, D. Magnetic Phase Diagram of Magnetoelectric $LiMnPO_4$. *Phys. Rev. B: Condens. Matter Mater. Phys.* **2012**, *85*, 224415.

(7) Vernay, F.; Penc, K.; Fazekas, P.; Mila, F. Orbital Degeneracy as a Source of Frustration in $LiNiO_2$. *Phys. Rev. B: Condens. Matter Mater. Phys.* **2004**, *70*, 014428.

(8) Sugiyama, J.; Ikedo, Y.; Mukai, K.; Nozaki, H.; Månsson, M.; Ofer, O.; Harada, M.; Kamazawa, K.; Miyake, Y.; Brewer, J. H.; Ansaldo, E. J.; Chow, K. H.; Watanabe, I.; Ohzuku, T. Low-temperature Magnetic Properties and High-temperature Diffusive Behavior of $LiNiO_2$ Investigated by Muon-spin Spectroscopy. *Phys. Rev. B: Condens. Matter Mater. Phys.* **2010**, *82* (22), 224412.

(9) Santoro, R. P.; Newnham, R. E. Antiferromagnetism in $LiFePO_4$. *Acta Crystallogr.* **1967**, *22* (3), 344−347.

(10) Kellerman, D. G.; Medvedeva, J. E.; Gorshkov, V. S.; Kurbakov, A. I.; Zubkov, V. G.; Tyutyunnik, A. P.; Trunov, V. A. Structural and Magnetic Properties of Orthorhombic Li_xMnO_2. *Solid State Sci.* **2007**, *9* (2), 196−204.

(11) Bie, X.; Gao, Y.; Yang, X.; Wei, Y.; Ehrenberg, H.; Hinterstein, M.; Chen, G.; Wang, C.; Du, F. Observation of the Second-order Magnetic and Reentrant Spin-glass Transitions in $LiNi_{0.5}Mn_{0.5}O_2$. *J. Alloys Compd.* **2015**, *626*, 150−153.

(12) Wills, A. S.; Raju, N. P.; Greedan, J. E. Low-Temperature Structure and Magnetic Properties of the Spinel $LiMn_2O_4$: A Frustrated Antiferromagnet and Cathode Material. *Chem. Mater.* **1999**, *11* (6), 1510−1518.

(13) Chernova, N. A.; Ma, M.; Xiao, J.; Whittingham, M. S.; Breger, J.; Grey, C. P. Layered $Li_xNi_yMn_yCo_{1-2y}O_2$ Cathodes for Lithium Ion Batteries: Understanding Local Structure via Magnetic Properties. *Chem. Mater.* **2007**, *19* (19), 4682−4693.

(14) Julien, C. M.; Ait-Salah, A.; Mauger, A.; Gendron, F. Magnetic Properties of Lithium Intercalation Compounds. *Ionics* **2006**, *12* (1), 21−32.

(15) Chernova, N. A.; Nolis, G. M.; Omenya, F. O.; Zhou, H.; Li, Z.; Whittingham, M. S. What Can We Learn about Battery Materials from Their Magnetic Properties? *J. Mater. Chem.* **2011**, *21* (27), 9865−9875.

(16) Padhi, A. K.; Nanjundaswamy, K.; Goodenough, J. B. d. Phospho-olivines as Positive-electrode Materials for Rechargeable Lithium Batteries. *J. Electrochem. Soc.* **1997**, *144* (4), 1188−1194.

(17) Whittingham, M. S. Ultimate Limits to Intercalation Reactions for Lithium Batteries. *Chem. Rev.* **2014**, *114* (23), 11414−11443.

(18) Rousse, G.; Rodriguez-Carvajal, J.; Patoux, S.; Masquelier, C. Magnetic Structures of the Triphylite $LiFePO_4$ and of Its Delithiated Form $FePO_4$. *Chem. Mater.* **2003**, *15* (21), 4082−4090.

(19) Lee, I. K.; Moon, S. J.; Shim, I.-B.; Kim, C. S. The Structural Transition and Magnetic Properties of Lithium Deintercalation in $LiFePO_4$. *IEEE Trans. Magn.* **2009**, *45* (10), 4268−4270.

(20) Mauger, A.; Zaghib, K.; Gendron, F.; Julien, C. M. Small Magnetic Polaron Effect in Lithium Iron Phosphates. *Ionics* **2008**, *14* (3), 209−214.

(21) Masrour, R.; Hlil, E. K.; Obbade, S.; Rossignol, C. Theoretical and Experimental Investigations of the Structural, Magnetic, Electronic, and Electrical Properties of Olivine $LiFePO_4$. *Solid State Ionics* **2016**, *289*, 214−219.

(22) Chen, J.; Vacchio, M. J.; Wang, S.; Chernova, N.; Zavalij, P. Y.; Whittingham, M. S. The Hydrothermal Synthesis and Characterization of Olivines and Related Compounds for Electrochemical Applications. *Solid State Ionics* **2008**, *178* (31−32), 1676−1693.

(23) Zboril, R.; Mashlan, M.; Petridis, D. Iron(III) Oxides from Thermal ProcessesSynthesis, Structural and Magnetic Properties, Mossbauer Spectroscopy Characterization, and Applications. *Chem. Mater.* **2002**, *14*, 969−982.

DOI: 10.1021/acs.jpclett.9b01557
J. Phys. Chem. Lett. 2019, 10, 4794−4799

(24) Panda, R. N.; Gajbhiye, N. S.; Balaji, G. Magnetic Properties of Interacting Single Domain Fe_3O_4 Particles. *J. Alloys Compd.* **2001**, *326* (1), 50−53.
(25) Salah, A. A.; Mauger, A.; Julien, C. M.; Gendron, F. Nano-sized Impurity Phases in Relation to the Mode of Preparation of $LiFePO_4$. *Mater. Sci. Eng., B* **2006**, *129* (1), 232−244.
(26) Molenda, J.; Marzec, J. Functional Cathode Materials for Li-ion Batteries u2014 Part II: $LiFePO_4$ and Its Composite. *Funct. Mater. Lett.* **2008**, *1* (02), 97−104.
(27) Herle, P. S.; Ellis, B.; Coombs, N.; Nazar, L. F. Nano-network Electronic Conduction in Iron and Nickel Olivine Phosphates. *Nat. Mater.* **2004**, *3* (3), 147−52.
(28) Chung, S.-Y.; Choi, S.-Y.; Yamamoto, T.; Ikuhara, Y. Atomic-scale Visualization of Antisite Defects in $LiFePO_4$. *Phys. Rev. Lett.* **2008**, *100* (12), 125502.
(29) Zaghib, K.; Mauger, A.; Goodenough, J. B.; Gendron, F.; Julien, C. Electronic, Optical, and Magnetic Properties of $LiFePO_4$: Small Magnetic Polaron Effects. *Chem. Mater.* **2007**, *19* (15), 3740−3747.
(30) Trimarchi, G.; Wang, Z.; Zunger, A. Polymorphous Band Structure Model of Gapping in the Antiferromagnetic and Paramagnetic Phases of the Mott Insulators MnO, FeO, CoO, and NiO. *Phys. Rev. B: Condens. Matter Mater. Phys.* **2018**, *97* (3), 035107.
(31) Zhang, W.; Yu, H.-C.; Wu, L.; Liu, H.; Abdellahi, A.; Qiu, B.; Bai, J.; Orvananos, B.; Strobridge, F. C.; Zhou, X.; et al. Localized Concentration Reversal of Lithium during Intercalation into Nanoparticles. *Sci. Adv.* **2018**, *4* (1), No. eaao2608.
(32) May, B. M.; Yu, Y.-S.; Holt, M. V.; Strobridge, F. C.; Boesenberg, U.; Grey, C. P.; Cabana, J. Nanoscale Detection of Intermediate Solid Solutions in Equilibrated Li_xFePO_4 Microcrystals. *Nano Lett.* **2017**, *17* (12), 7364−7371.
(33) Aaboubi, O.; Lòs, P.; Amblard, J.; Chopart, J. P.; Olivier, A. Electrochemical Investigations of the Magnetic Field Influence on Mass Transport toward an Ultramicrodisk. *J. Electrochem. Soc.* **2003**, *150* (2), No. E125.
(34) Ragsdale, S. R.; Grant, K. M.; White, H. S. Electrochemically Generated Magnetic Forces. Enhanced Transport of a Paramagnetic Redox Species in Large, Nonuniform Magnetic Fields. *J. Am. Chem. Soc.* **1998**, *120*, 13461−13468.
(35) Ragsdale, S. R.; Lee, J.; Gao, X.; White, H. S. Magnetic Field Effects in Electrochemistry. Voltammetric Reduction of Acetophenone at Microdisk Electrodes. *J. Phys. Chem.* **1996**, *100*, 5913−5922.

DOI: 10.1021/acs.jpclett.9b01557
J. Phys. Chem. Lett. 2019, 10, 4794−4799